Journal of Colloid and Interface Science 608 (2022) 2321–2329

Contents lists available at ScienceDirect

Journal of Colloid and Interface Science

journal homepage: www.elsevier.com/locate/jcis

Examining the role of salinity on the dynamic stability of Pickering emulsions

Daniel Hatchell *, Wen Song, Hugh Daigle

Hildebrand Department of Petroleum and Geosystems Engineering, University of Texas at Austin, 200 E Dean Keeton St, Austin, TX 78712, USA

GRAPHICAL ABSTRACT

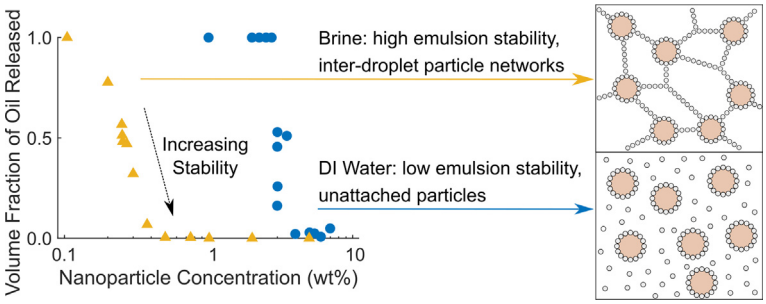

ARTICLE INFO

Article history:
Received 26 March 2021
Revised 23 October 2021
Accepted 25 October 2021
Available online 6 November 2021

Keywords:
Nanoparticles
Pickering emulsions
Dynamic stability
Centrifugation

ABSTRACT

Hypothesis: The effect of salinity on Pickering emulsion stability to coalescence under dynamic forces present during flow in porous media for applications including enhanced oil recovery is poorly understood. Recent work suggests the absence of significant electrostatic repulsion in brine prompts unattached particles to assemble into inter-droplet networks that increase emulsion stability. We hypothesize that emulsions stabilized by nanoparticles coated with (3-glycidyloxypropyl)trimethoxysilane (GLYMO) will generate particle networks in brine and exhibit greater stability to coalescence than in deionized water (DI).

Experiments: We stabilized decane-in-water emulsions with GLYMO-coated silica nanoparticles at various particle concentrations using brine and DI as the aqueous phase. We imaged the emulsions to calculate droplet diameters, then centrifuged the emulsions and weighed the volume of decane released to determine the extent of coalescence. We compared these measurements to evaluate the effect of salinity on emulsion stability.

Findings: Emulsions demonstrate greater dynamic stability and smaller droplet diameters with increasing nanoparticle concentration and salinity. Controlling for differences in droplet size, we observe that brine reduces the emulsion coalescence rate by a factor of 78 ± 23 relative to DI. This difference supports and quantifies past work suggesting that unattached nanoparticles aggregate in brine and increase overall emulsion stability, whereas nanoparticles in DI remain separated.

1. Introduction

Solid-stabilized emulsions (i.e., Pickering emulsions) have seen increased focus in literature [1–4] as a potential alternative to surfactant-stabilized emulsions for applications such as enhanced

* Corresponding author.
E-mail address: dchatchell@utexas.edu (D. Hatchell).

https://doi.org/10.1016/j.jcis.2021.10.154
0021-9797/

oil recovery [5,6] and aquifer decontamination [7]. Solid particles stabilize emulsions by attaching to droplet surfaces through interfacial adsorption [8,9]. The particles adsorb to a fluid–fluid interface with high attachment energies and sterically prevent coalescence between adjacent droplets [10,11]. The attachment energy is high enough to stabilize macroemulsions (emulsions with droplets>1 μm), a property that makes Pickering emulsions well suited for both conformance-controlled [12,13] and mobility-controlled [14] flow through porous media, particularly in harsh conditions [15].

The attachment energy is the product of the area a particle occupies at the interface by the surface tension of the two phases, given in Eq. (1) for an oil–water emulsion [11]:

$$\Delta E = \pi r^2 \gamma_{OW}(1 - |cos(\theta_{OW})|)^2 \quad (1)$$

where ΔE is the change of energy of the particle transferring from the bulk to the surface, r is the particle radius, γ_{OW} is the oil–water interfacial tension, and θ_{OW} is the oil–water contact angle on the particle surface. The static stability of an emulsion is determined by the attachment energy of its particles. A nanoparticle with intermediate wettability (θ_{OW} = 90°) will achieve the highest ΔE and generate the most statically stable emulsions. Static stability can be controlled by manipulating the particle surface and changing the contact angle; various types of particles have been statically stabilized by this method [15–21]. Eq. (1) is not suitable for predicting stability of a flowing emulsion, however. During flow through porous media, there are more complicated dynamic forces present influencing stability to coalescence. Pickering emulsion stability under dynamic conditions is more difficult to determine and not as well understood.

Dynamic stability is typically measured with either centrifugation [22–26] or rheometry [27,28]. Griffith and Daigle [22] demonstrated that an emulsion's stability to coalescence in a centrifuge was an accurate indicator of its dynamic stability during flow. They generated decane-in-water emulsions stabilized by silica nanoparticles coated with [3-(2,3-dihydroxypropoxy)propyl]-trimethoxysilane (GLYMO), centrifuged the emulsions, and calculated a critical demulsification pressure – the pressure necessary to initiate partial coalescence of the emulsion. They compared these pressures to observations of the coalescence of emulsions flowing through a glass capillary tube, and found them to be good predictors of dynamic stability. Using these methods, some general factors that influence Pickering emulsion dynamic stability have been found. Emulsions with smaller droplet diameters, greater concentrations of nanoparticles, and particles with more intermediate wettability have all been shown to exhibit greater dynamic stability under certain conditions [22–28]. Dynamic stability also appears to increase with increasing salinity [22,24,27–30]. Investigating the role of salinity, Whitby et al. [28] examined the effect of shear force on coalescence in bromohexadecane-in-water Pickering emulsions while altering the concentration of sodium chloride. Using confocal fluorescence images, they demonstrated the tendency for unattached particles in the aqueous phase to aggregate around droplets at increased salinity, accompanied by increasing particle dispersion viscosity and emulsion stability. They were successfully able to destabilize emulsions by applying shear. Their work supported other studies suggesting the formation of inter-droplet particle networks in the aqueous phase of high-salinity emulsions [31–34]. These networks are thought to be rigid enough to prevent droplets from approaching and coalescing, and could play a significant role in stabilizing emulsions during flow through porous media.

While particle networks have been qualitatively observed, there is little work in literature attempting to quantify their impact on coalescence in response to compressive stress while controlling for droplet size and nanoparticle concentration. The objective of this work is to quantify the effect of salinity on emulsion formation and coalescence under dynamic conditions with detailed measurements while controlling for droplet size and nanoparticle concentration. We generated and centrifuged emulsions over a range of nanoparticle concentrations and tracked differences in droplet diameter to isolate the effect of salinity. We then combined our observations with calculations of inter-particle forces to infer the presence and impact of inter-droplet particle networks.

2. Materials and methods

2.1. Materials

NexSil 6 silica nanoparticles were obtained from Nyacol as a nanoparticle core for functionalization. These particles, nominally 6 nm in diameter, have a reported diameter range of 5–7.5 nm and a specific surface area range of 340–545 m^2/g. The specific stock used contained 18.8 wt% nanoparticles. (3-glycidyloxypropyl)trimethoxysilane (GPTMS or Ring-Closed GLYMO) was purchased from Sigma-Aldrich (>98% purity). *n*-decane was obtained from Chevron Phillips (>99% purity). Sodium chloride (NaCl), calcium chloride ($CaCl_2$), and 12.1 N hydrochloric acid (HCl) were purchased from Fischer Scientific. A Barnstead E-Pure Ultrapure Water Purification System generated 18.2 MΩ·cm deionized water (DI) for use in all experiments.

2.2. Functionalization of Ring-Opened GLYMO nanoparticles

The procedure to functionalize silica nanoparticles with Ring-Opened GLYMO was similar to previous work [22,34,35]. A batch of NexSil 6 stock solution containing 2 g nanoparticles was slightly diluted with DI in a cylindrical vial. 0.03 N HCl, diluted from a 12.1 N stock, was mixed with 4.4 g of methanol in a beaker to give a mixture with a resulting molarity of 0.01 M HCl. Ring-Closed GLYMO was added to the beaker such that there were 5 μmol in solution per m^2 of nanoparticle area based on an average surface area of 445 m^2/g, and stirred for a few minutes to open the epoxy ring and form Ring-Opened GLYMO ([3-(2,3-dihydroxypropoxy)propyl]-trimethoxysilane, referred to from here simply as GLYMO). This GLYMO mixture was then added dropwise to the vial containing 2 g of nanoparticles. The vial was sealed with PTFE tape and stirred overnight at 65° C to graft GLYMO onto the silica surface via hydrolysis condensation. Following the reaction, the mixture was opened to air to allow the methanol to evaporate. The resulting dispersion – approximately 17 g total - was purified in Amicon Ultra-15 30 K MWCO centrifugal filters by centrifuging eight times with DI at 5000 g for 30 min. The separated particles after this process were redispersed in DI by sonication. The success of filtration was verified by measuring the surface tension of the aqueous particle dispersion with via the pendant drop method in a Ramé-Hart goniometer. The final, filtered dispersion of GLYMO-functionalized nanoparticles (GLYMO-NP) was used for experiments. Multiple batches were prepared by this method.

2.3. Nanoparticle characterization

Nanoparticle hydrodynamic diameter and zeta potential were measured with a Malvern Zetasizer Nano ZS. Diameter measurements were taken as the z (intensity) average and number average diameter of a 1 wt% nanoparticle dispersion in a cuvette, both as reported by the Zetasizer. The zeta potential was measured from a 1 wt% nanoparticle dispersion in a DTS 1070 zetacell. These two measurements were carried out with unfiltered particles.

The coverage of GLYMO molecules on the silica surface was quantified in a Mettler Thermogravimetric Analyzer TGA/DSC 1

using thermogravimetric analysis (TGA). Similar to previous studies [33,35], samples of filtered GLYMO-NP were placed in an alumina crucible and dried overnight in an oven at 80 °C to remove water with the goal of leaving 5 mg of dry sample. TGA measurements were performed by ramping temperature from 30 °C to 110 °C at a rate of 10 °C/min, holding at 110 °C for 20 min to remove residual water, and then ramping up to 800 °C. The percent of organic mass, an indicator of how much GLYMO attached to the silica nanoparticles, was taken as the fraction of mass lost ramping temperature from 110 °C to 800 °C.

2.4. Emulsion generation

Oil-in-water emulsions were prepared by combining 20 mL of *n*-decane with 20 mL of aqueous nanoparticle dispersion in a 50 mL glass beaker. The filtered GLYMO-NP dispersions were diluted in either DI or brine to reach a desired nanoparticle concentration ranging from 0.1 wt% to 7 wt%, depending on the experiment. We formulated brine based on the ions and ionic ratios specified by the American Petroleum Institute [36] (i.e., "API brine"). Our "5API brine" (containing 5 wt% total dissolved solids, rather than the traditional 10 wt%) was prepared by mixing NaCl and $CaCl_2$ at a four-to-one mass ratio with DI, such that nanoparticles were ultimately dispersed in a 4 wt% NaCl, 1 wt% $CaCl_2$ aqueous phase. We refer to GLYMO-NP emulsions in DI and in 5API brine as GLYMO-NP-DI and GLYMO-NP-5API emulsions, respectively. The mixtures were emulsified via sonication in a 30 W Branson Digital Tip Sonifier using a 5 mm microtip. The sonifier was set to 50% amplitude with the tip positioned at the oil–water interface and run for 10 s. The mixture was then stirred and the process was repeated two more times, by which point each sample had fully emulsified.

2.5. Centrifugation

30 g of emulsion was added to a Falcon 50 mL Polypropylene Conical Tube. The tube was centrifuged in an Eppendorf 5810R Centrifuge at 5000 g of acceleration for 15 min, matching parameters from previous work [22]. Centrifugation caused three phases to form in the tube: a top phase of released decane, a middle phase of concentrated emulsion, and a bottom aqueous phase. For strong emulsions, the top and bottom phases could be negligible or absent; similarly, weak emulsions exhibited only a trace emulsion phase in the middle. Released decane from centrifugation was quickly separated from the top of each sample with a pipette and the mass difference was measured on a scale to determine the extent of coalescence.

2.6. Microscope imaging and droplet size calculation

Emulsions were imaged using a Nikon Labophot-Pol microscope and Nikon Digital Sight DS-Fil camera. 40 μL of emulsion, diluted in the appropriate solution (brine or DI), was placed onto a microscope slide under a cover slip. Microscope images were taken at scales of 40x, 10x, and 4x zoom and analyzed by ImageJ to calculate droplet areas. Droplet diameters were determined from the dataset of droplet areas by calculating the geometry of the droplets and accounting for a cover slide height of 50 μm (most droplets had a diameter of below 50 μm and were therefore assumed to be spherical). Emulsion droplet sizes were reported as the Sauter diameter, D_{32}, which is a volume-weighted measure of average droplet size:

$$D_{32} = \frac{\sum_i^n D_i^3}{\sum_i^n D_i^2} \tag{2}$$

where D_i refers to the diameter of the i^{th} droplet in a set of n total droplets.

3. Results and discussion

3.1. Nanoparticle characterization

We characterized the GLYMO-NP and compared them to bare NexSil 6 particles to verify the extent of the grafting reaction. With DLS, we measured the z-average particle diameter, number-average diameter, and zeta potential. With TGA, we measured the organic fraction and calculated a surface coverage fraction and nanoparticle mass. Surface tension was measured with the pendant-drop method. These properties are reported in Table 1.

The coverage fraction from TGA was calculated by the following equation, modified from Worthen, et al [35]:

$$\varphi_l = \frac{f_o - f_{o,np}}{(1 - f_o - f_i + f_{o,np}) S_A M_{TGA} N_{SiOH}} \tag{3}$$

In Eq. (3), φ_l refers to the surface coverage of ligand as a dimensionless fraction ranging from 0 (no coverage) to 1 (full coverage). S_A is the specific surface area of the nanoparticle core (445 m^2/g for NexSil 6), M_{TGA} is the molecular weight GLYMO removeable by TGA (133.17 g/mol) [35], and N_{SiOH} is the density of silanol sites available for GLYMO grafting at the silica surface (assumed to be 4.6 sites/nm^2) [37]. The values f_o, f_i, and $f_{o,np}$ represent different mass fractions of the particle relevant to TGA. The organic fraction of the particle, f_o, is the fraction of the particle mass that is removed at high temperatures during TGA. The organic fraction of the original nanoparticle core, $f_{o,np}$, is the same measurement for bare silica, and is subtracted from f_o to control for mass loss at the bare silica surface during TGA. The inorganic fraction, f_i, is the mass of GLYMO added to the NexSil 6 particle but not removed by TGA.

The calculated surface coverage, 0.33, is consistent with values of 0.38 and 0.35 reported by Worthen, et al. [35], and 0.32 reported by Griffith and Daigle [33] for NexSil 6 particles coated with GLYMO by similar processes. The TGA mass-temperature curves are plotted in Fig. S1. These characterizations altogether were good indicators that GLYMO had successfully grafted to the silica surface.

We finally measured the surface tension of a 1 wt% GLYMO-NP dispersion in deionized water with the pendant drop method to verify the success of particle filtration. The measured value of 69.22 ± 0.17 mN/m was only slightly less than that of pure water (72 mN/m). We further demonstrate successful filtration by comparing centrifugation experiments of unfiltered and filtered particles in Fig. 4.

Table 1
GLYMO-nanoparticle parameters measured with DLS and TGA.

	Bare NexSil 6	GLYMO-NP
Z average diameter (nm)	16.31	15.19
Number average diameter (nm)	4.65	6.44
Polydispersity Index	0.218	0.466
Zeta Potential (mV)	−46 ± 6	−43 ± 6
Organic fraction removed by TGA (f_o)	0.024	0.145
Surface coverage fraction of GLYMO (φ)	0.00	0.33
Estimated mass of single particle (g)	2.5×10^{-19}	3.0×10^{-19}
Surface tension of 1 wt% filtered particle dispersion (mN/m)	n/a	69.22 ± 0.17

3.2. Evaluation of nanoparticle interactions with extended DLVO theory

We can further characterize the properties and interactions of GLYMO-NP using extended DLVO theory [35,38,39]. The original DLVO theory, named for Derjaguin, Landau, Verwey, and Overbeek [40,41], describes the behavior of dispersed particles subject to van der Waals attraction and electrostatic forces. The potential energy (Φ) from van der Waals attraction between two GLYMO-NP is given by the Derjaguin approximation [42]:

$$\Phi_{wdV}(d) = -\frac{(r+l)\left(\sqrt{A_m}-\sqrt{A_p}\right)^2}{12d} \tag{4}$$

where r is the particle core radius and l is the ligand length, assumed for GLYMO to be 0.95 nm [43]. A_m and A_p are the Hamaker constants for the continuous phase and the particle, respectively. We used Hamaker constants of 3.7 × 10^{-20} J for the fluid and 6.3 × 10^{-20} J for the particles, taken from Worthen et al. [35]. The core-to-core separation distance is given by d. Van der Waals attraction between the particles yields a highly negative interaction energy at short distances that approaches zero as distance increases. We assume that this force is not affected by ionic concentration. Electrostatic repulsion can be approximated by Eq. (5) [42]:

$$\Phi_R(d) = 32\pi r\varepsilon_o\varepsilon_r\left(\frac{k_BT}{e}\right)^2 tanh^2\left(\frac{e\Psi_o}{4k_BT}\right)e^{-\kappa d} \tag{5}$$

where T is temperature (equal to 298 K for room temperature), k_B is Boltzmann's constant, and Ψ_o is the surface potential of the particle, assumed to be equal to the zeta potential. ε_o and ε_r are the permittivity of free space and the relative permittivity of the aqueous phase, respectively. The latter term is given for a NaCl/$CaCl_2$ mixture in Eq. (6), following the approach by Chen and Panagiotopoulus [44]:

$$\begin{aligned}\varepsilon_r = {} & \left[\varepsilon_{rw} - 16.2c_{NaCl} + 3.1{c_{NaCl}}^{2/3}\right] * \left(1 - \frac{3c_{CaCl2}}{2c_{NaCl}+3c_{CaCl2}}\right) \\ & + \left[\varepsilon_{rw} - 11.3c_{CaCl2} + 1.9{c_{CaCl2}}^{2/3}\right] * \left(\frac{3c_{CaCl2}}{2c_{NaCl}+3c_{CaCl2}}\right)\end{aligned} \tag{6}$$

The parameters c_{NaCl} and c_{CaCl2} refer to the molar concentrations of NaCl and $CaCl_2$, respectively, and ε_{rw} is the relative permittivity of pure water. Altogether, we calculate a relative permittivity of 61.2 for 5API brine. The inverse Debye length, κ, is given by Eq. (7) [42]:

$$\kappa = \sqrt{\frac{\sum_i \rho_{\infty,i}e^2z_i^2}{\varepsilon_o\varepsilon_r k_BT}} \tag{7}$$

The inverse Debye length is calculated as a function of the number density of ion species i in the bulk solution, $\rho_{\infty,i}$, the species valency, z_i, and the elementary charge, e (as well as k_B, T, ε_o, and ε_r from before). We assume that DI has an NaCl concentration of 0.01 mM, giving an inverse Debye length of κ = 0.0104 nm^{-1}; 5API brine, in contrast, gives an inverse Debye length of κ = 3.80 nm^{-1}.

By the above equations, electrostatic repulsion is some finite, positive value at a separation distance of zero and decreases with increasing distance. The rate that electrostatic repulsion decays is controlled by the Debye length, which itself depends on ionic concentration. In DI, electrostatic repulsion decays slowly with distance, but in 5API brine, due to ionic screening of electrostatic charges, electrostatic repulsion decays almost immediately. As a result, electrostatic repulsion is significant in DI and assumed to be zero in brine. Extended DLVO theory combines these two forces with steric interactions between GLYMO molecules at the silica surface [35]. Steric interaction Φ_s is modeled as two components: an osmotic contribution, Φ_o, and an entropic/elastic contribution, Φ_e [45]:

$$\Phi_s = \Phi_o + \Phi_e \tag{8}$$

The osmotic component of steric energy is described by Eq. (9):

$$\begin{aligned}\Phi_o(d) &= 0 \quad d \geq 2l \\ \Phi_o(d) &= \frac{4\pi r\varphi^2(0.5-\chi)}{v_1}\left[1-\frac{d}{2}\right]^2 l \quad l \leq d < 2l \\ \Phi_o(d) &= \frac{4\pi r\varphi^2(0.5-\chi)l^2}{v_1}\left[\frac{d}{2l}-\frac{1}{4}-\ln\left(\frac{d}{l}\right)\right] \quad d < l\end{aligned} \tag{9}$$

Eq. (9) is a piecewise function of d, the distance measured from the surface of the nanoparticle core. The domain intervals are defined by the ligand length, l, assumed to be 0.95 nm [43]. φ is the volume coverage fraction of GLYMO at the silica particle surface, χ is the Flory-Huggins interaction parameter, and v_1 is the volume of one GLYMO molecule at the surface. Following the work of Worthen et al. [35], we used a Flory-Huggins parameter of 0.1 for our calculations, representing good compatibility between the GLYMO ligands and aqueous phase. The entropic/elastic component of steric energy is calculated by another piecewise function:

$$\begin{aligned}\Phi_e(d) &= 0 \quad d \geq l \\ \Phi_e(d) &= \frac{2\pi r N_a\varphi d^2\rho_p l^2}{M_w}\left[\frac{d}{l}\ln\left(\frac{d}{4l}\left(3-\frac{d}{l}\right)^2\right) - 6\ln\left(\frac{3-d/l}{2}\right) + 3\left(1-\frac{d}{l}\right)\right] \quad d < l\end{aligned} \tag{10}$$

The parameters ρ_p and M_w refer to the density of bulk GLYMO and the molecular weight of GLYMO, respectively. At a separation distance close to zero, the total steric repulsion generates a high interaction energy; this energy decreases with increasing distance and equals zero at a distance of 1.9 nm (equal to twice the estimated length of a GLYMO molecule, at which point two particles are no longer in contact). The steric repulsion does not significantly change with a change in ionic concentration of the aqueous phase. Finally, the total interaction energy Φ_T is calculated by combining the van der Waals, electrostatic, and steric terms:

$$\Phi_T = \Phi_{vdW} + \Phi_R + \Phi_s \tag{11}$$

Fig. 1 plots the interaction energies in dimensionless thermal units (E/k_BT) of GLYMO-NP in 5API brine and GLYMO-NP in DI as a function of separation distance between particle cores.

Fig. 1(a) plots the DLVO interaction energies of GLYMO-NP in DI. These energies are always positive within the domain of interest, suggesting that particles will repel in dispersion. Fig. 1(b) displays the DLVO interaction energies of GLYMO-NP in brine. With electrostatic repulsion absent, the total interaction energy is a sum of the steric and van der Waals forces. Although this energy is strongly negative at near-zero separation distance, the peak observed at approximately 0.1 nm of separation is sufficient to prevent particles from coming into contact and aggregating. Without GLYMO grafted to the surface, these particles would only exhibit van der Waals attraction and therefore be unstable in brine.

3.3. Emulsion imaging

To validate our procedure for imaging droplets at different microscope scales and compiling the images into a single D_{32} diameter, we separately generated four 0.25 wt% GLYMO-NP emulsions in 5API brine and independently imaged each batch. A combined histogram of the measured droplet distributions of these four emulsions is plotted in Fig. 2, alongside microscope images showing a representative sample of the emulsion at the largest (40x) and smallest (4x) zoom lengths. The individual histograms and intermediate zoom scale are displayed in Fig. S2.

The four batches that comprise the histogram in Fig. 2 (a) all fell within a similar range. They exhibited D_{32} diameters of 30 ± 4 μm,

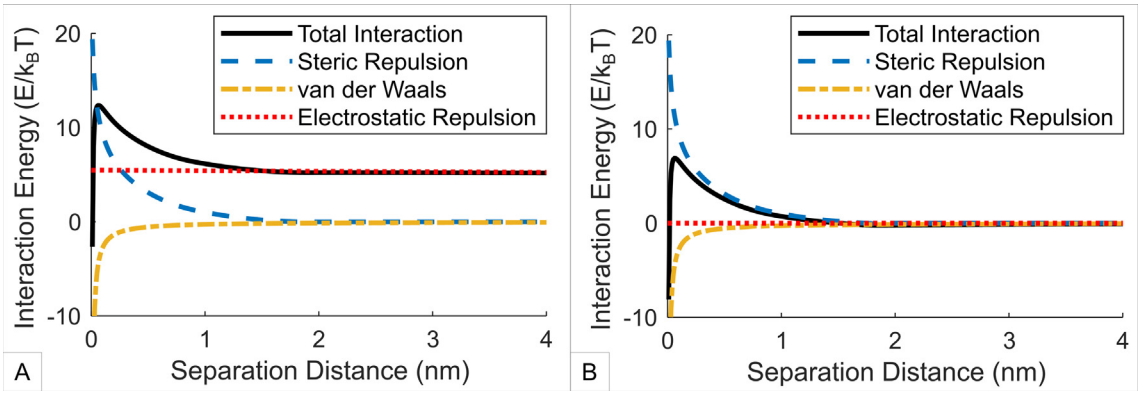

Fig. 1. (a) DLVO interactions of GLYMO-NP in DI as a function of core surface to core surface particle separation distance, assuming significant electrostatic repulsion; (b) DLVO interactions of GLYMO-NP in 5API brine as a function of separation distance, where electrostatic repulsion is assumed to be zero.

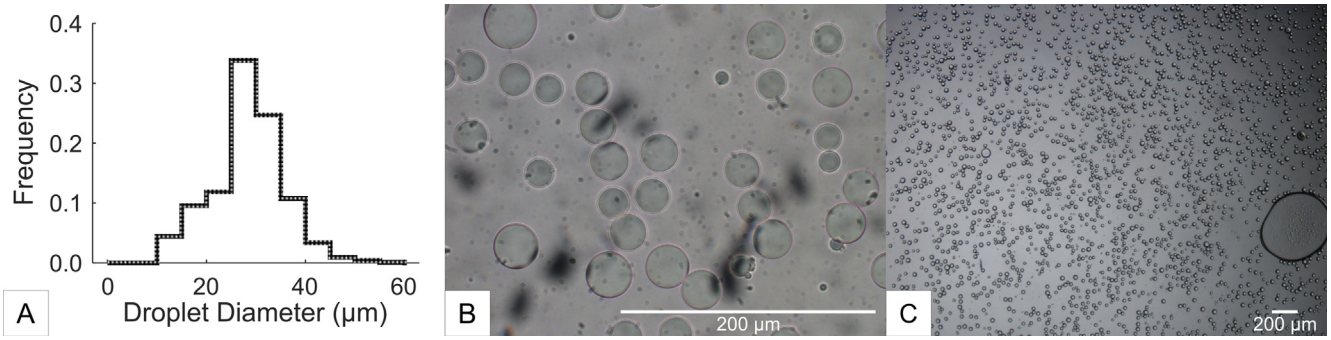

Fig. 2. (a) Representative histogram of droplet size distributions of 0.25 wt% GLYMO-NP-5API emulsions. The frequency of droplets at each diameter bin has been normalized to sum to a value of one. Images (b) and (c) show the same 0.25 wt% GLYMO-NP-5API emulsion sample on a microscope slide imaged at 40x and 4x zoom.

31 ± 2 μm, 32 ± 3 μm, and 31 ± 2 μm, respectively. These results help demonstrate the repeatability of the emulsion generation and imaging process.

Two emulsion series were prepared for imaging and centrifugation: GLYMO-NP emulsion in DI and GLYMO-NP emulsion in 5API brine. Each emulsion series contained a wide range of nanoparticle concentrations to observe the effect on emulsion stability and droplet size, and identify any changes between DI and 5API brine. Fig. 3 plots the D_{32} diameters of the DI and 5API brine emulsion series in microns against nanoparticle mass concentration on a log–log scale. Error bars are given as a propagated measurement error of ± 1 pixel of droplet diameter for each droplet in the D_{32} calculation.

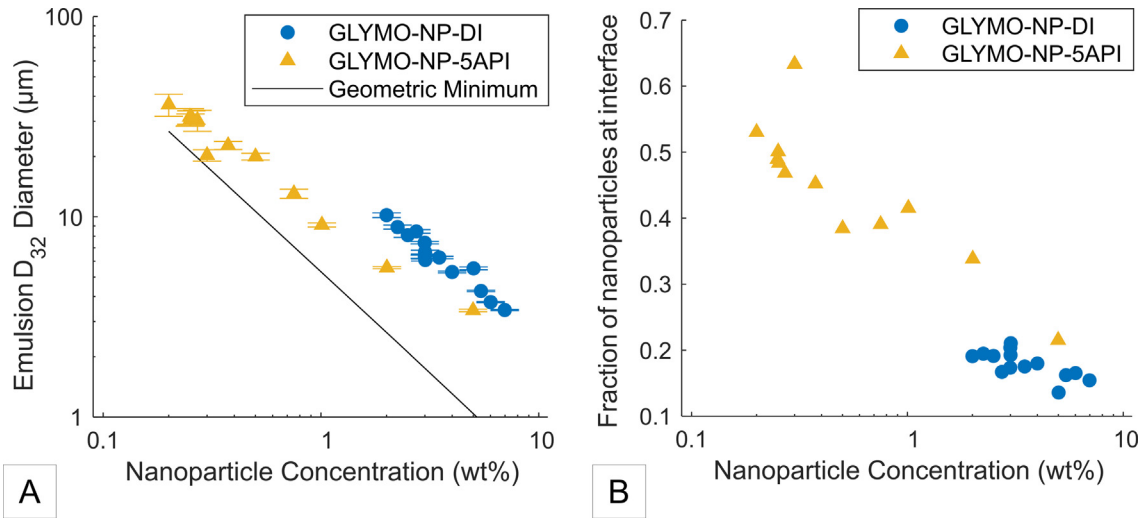

Fig. 3. **(a)** D_{32} diameters of GLYMO-NP-DI and GLYMO-NP-5API emulsions as a function of nanoparticle concentration in the original aqueous phase. The geometric minimum line is an estimate of the smallest possible droplet size given the quantity of nanoparticles available to stabilize an emulsion; (b) Estimated fraction of nanoparticles at the surface of a droplet as a function of nanoparticle mass concentration in the aqueous phase.

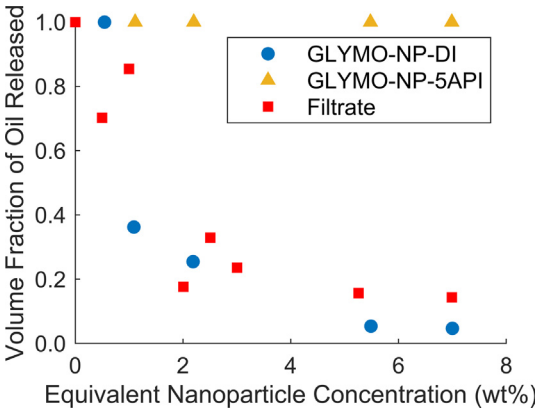

Fig. 4. Volume fraction of oil released during centrifugation for unfiltered GLYMO-NP-DI and GLYMO-NP-5API emulsions as a function of nanoparticle mass concentration. The filtrate concentration is converted into an equivalent nanoparticle concentration for comparative purposes.

GLYMO-NP proved capable of stabilizing smaller, more statically stable emulsion droplets in 5API brine than in DI for the same initial concentration of nanoparticles. As GLYMO-NP concentration increased from 0.2 wt% to 5 wt% in the aqueous phase, the D_{32} diameters of GLYMO-NP-5API emulsions decreased from 36 ± 5 μm to 3.41 ± 0.05 μm. A brine emulsion was attempted at 0.1 wt% nanoparticles, but it was not strong enough to remain stable under static conditions. This observation indicates that the critical concentration for stability of GLYMO-NP-5API emulsion lies between 0.1 and 0.2 wt%. GLYMO-NP-DI emulsions generated larger droplets that were only statically stable at higher nanoparticle concentrations. Ranging from 2 wt% to 7 wt% nanoparticle concentration in the aqueous phase, the D_{32} diameters of GLYMO-NP-DI emulsions decreased from 10.2 ± 0.3 μm to 3.42 ± 0.02 μm. Another DI emulsion was attempted at 1 wt% nanoparticles, but it too did not remain stable at static conditions, indicating that the critical concentration for stability of GLYMO-NP-DI emulsion is between 1 and 2 wt%. Holding concentration constant, GLYMO-NP-DI emulsions had 50–80% larger droplet sizes. Because larger emulsion droplets are expected to be less stable than equivalent smaller droplets [28,46], it was not surprising that GLYMO-NP-5API emulsion exhibited greater static stability at the same nanoparticle concentration; however, the apparently higher stability of GLYMO-NP-5API emulsion at lower nanoparticle concentrations (when droplet sizes were much higher) suggested a fundamental difference between the two emulsions. We investigated this difference in section 3.4 with dynamic centrifugation experiments.

The geometric minimum line representing the minimum droplet diameters expected for a given weight fraction of nanoparticles is plotted in Fig. 3(a). This line corresponds to the droplet size associated with the maximum surface area that the nanoparticles could occupy if every particle in the dispersion was attached to an oil–water interface. For this calculation, we assumed that the particles exhibited hexagonal packing at the interface in a dense monolayer with a diameter of 7.9 nm (the nominal diameter of NexSil 6 plus twice the expected length of a GLYMO molecule). Both the 5API brine and DI series displayed larger droplet diameters than the geometric minimum – an indication that some fraction of the nanoparticles migrated to an interface, but another significant portion remained dispersed in the aqueous phase. This difference was greater at higher nanoparticle concentrations; while the geometric minimum line, by definition, can be fit to an exponential curve with an exponent of −1.0, both the 5API brine and DI curves were best fitted with an exponent of −0.8, suggesting less efficient migration of particles during sonication at higher particle concentrations. Given their smaller diameters at equal concentration, GLYMO-NP-5API emulsions exhibited more particles at an interface than the GLYMO-NP-DI emulsions, evidence that particles sonicated more efficiently in brine than in DI. Fig. 3 (b) plots the estimated fraction of particles at the surface of a droplet as a function of nanoparticle mass concentration, calculated from these results.

The more efficient migration of particles to the interface during sonication in brine can be explained by extended DLVO theory. As seen in Fig. 1(b), GLYMO-NP have sufficiently high total interaction energies at distances up to twice the ligand length to sterically repel other particles and prevent aggregation, despite the absence of electrostatic forces. Beyond the range of steric repulsion, however, the total interaction energy is small and slightly negative. The GLYMO-NP do not repel further than short distances in brine and may even loosely pack together. During sonication, these particles may form dense monolayers at the oil–water interface more easily. Because they migrate to the interface more efficiently, a greater fraction of particles ends up situated at a droplet surface after sonication. The particles stabilize a higher surface area of a finite volume of decane, resulting in smaller droplets. GLYMO-NP form dense monolayers less easily when migrating to an interface in DI. Due to the presence of electrostatic repulsion, as plotted in Fig. 1(a), particles require more energy to approach and pack together at the surface. This tendency prevents as many nanoparticles from situating at a droplet surface after sonication, resulting in less surface area of decane stabilized and consequently larger droplets. The deviation from the minimum lines at higher nanoparticle concentrations in both DI and 5API brine indicated even less efficient sonication as more particles are added to dispersion.

3.4. Centrifugation

To measure the dynamic stability of each emulsion, a centrifuge was used to apply a constant acceleration of 5000 g for 15 min to an emulsion to quantify the effect of dynamic force on emulsion coalescence. Following centrifugation, each emulsion separated into three distinct phases. The bottommost layer was an aqueous phase, containing either DI or brine with no decane droplets. This phase likely also contained some number of dispersed nanoparticles, unattached to an oil–water interface. The central layer was a dense, highly-creamed emulsion phase, consisting of multiple decane droplets surrounded by a thin film of the continuous phase (either DI or brine). This central layer was sampled for microscope imaging before and after centrifugation to determine the average droplet size. The uppermost layer was an oleic phase, containing decane released by droplet coalescence events. The volume of this uppermost phase was extracted and measured to determine the fraction of emulsion coalesced, a proxy for emulsion stability. The three phases are illustrated in Fig. S3. In the case that the emulsion had almost entirely coalesced with only trace amounts of the central layer remaining, the volume fraction was reported as 1. If the uppermost layer was too small to extract with a pipette, the volume fraction was reported as 0.

We first examined the centrifugation behavior of unfiltered GLYMO-NP-DI and GLYMO-NP-5API emulsions to contrast their behavior and to demonstrate the successful filtration of our filtered particles. Fig. 4 displays the volume fraction of oil released during centrifugation against nanoparticle concentration for emulsions generated with unfiltered particles, as well as emulsions generated from the filtrate of filtered particles.

We assumed that the filtrate had the same chemical composition of the aqueous phase of unfiltered particles. Using the unfiltered GLYMO-NP stock as a basis, we converted this chemical composition into an equivalent nanoparticle mass concentration (essentially, the quantity of unfiltered aqueous phase associated

with a given quantity of GLYMO-NP). Unfiltered GLYMO-NP-DI emulsion closely tracked the stability behavior of the filtrate-stabilized emulsion, coalescing easily in the centrifuge at low nanoparticle concentrations but quickly demonstrating high stability as nanoparticle concentration increased to 5–7 wt%. Unlike the emulsions with filtered particles that will be presented in Fig. 5, unfiltered GLYMO-NP-DI emulsion exhibited a more gradual decline in stability. There was no critical concentration range for the unfiltered emulsion, and even at low nanoparticle concentrations of 1 wt%, the unfiltered GLYMO-NP-DI emulsion still only partially coalesced in the centrifuge (the filtered GLYMO-NP-DI emulsion was not even statically stable at 1 wt% nanoparticle concentration). On the other hand, unfiltered GLYMO-NP-5API emulsions were completely unstable at even static conditions.

Fig. 5(a) plots the volume fraction of oil released during centrifugation against nanoparticle concentration for filtered GLYMO-NP-DI and GLYMO-NP-5API emulsions. Fig. 5(b) plots the same volume fraction against emulsion D_{32} diameter in microns (similar to Fig. 3, error bars are given as ± 1 pixel of measurement error in the individual droplet diameters propagated through the D_{32} diameter calculation). The shaded regions represent uncertainty in the volume fraction of oil released. This uncertainty is equal to two standard deviations of the repeated values of 3 wt% GLYMO-NP-DI emulsion and 0.25 wt% GLYMO-NP-5API emulsion, respectively, and is centered about a linear fit to the data.

Both GLYMO-NP-DI and GLYMO-NP-5API emulsions followed a similar trend, releasing a high volume fraction of decane at low nanoparticle mass concentrations, showing an increase of stability across a critical concentration range, and releasing almost no decane at sufficiently high concentrations. Much of the transition between instability and stability for GLYMO-NP-5API emulsions occurred between 0.2 wt% and 0.375 wt% nanoparticles. A similar transition between 2.75 wt% and 4 wt% nanoparticles was observed for GLYMO-NP-DI emulsions. Approximately 12 times more nanoparticles were required to stabilize the emulsions in DI than in 5API brine. GLYMO-NP-5API emulsion also produced a smoother stability curve with less scatter, indicating a more repeatable stability mechanism.

Because droplet diameter is understood to influence the stability of emulsions [28,46], comparing nanoparticle concentrations directly does not give a complete picture of the difference in emulsion stability. Fig. 5(b) plots the same volume fraction data from Fig. 5(a) as a function of droplet size to account for this difference. The shaded regions again represent two standard deviations of uncertainty in the volume fraction of oil released, centered around a linear fit to the data. Controlling for droplet size, the GLYMO-NP-DI emulsions still coalesced more easily in the centrifuge. The DI emulsions transitioned from stable to unstable at a D_{32} diameter range of 4.3 ± 0.5 times lower than the GLYMO-NP-5API emulsions. Notably, the process of centrifugation did not significantly affect the measured D_{32} diameter for any emulsion. No emulsions exhibited a significant change in D_{32} diameter measured before or after centrifugation. This finding suggests that – after some initial coalesce – droplets coalesced with the bulk separated decane at the top of the centrifuge vial, rather than with other droplets. This outcome is reasonable for a centrifuge system because the compressive force is strongest at the top of the vial.

The observation that emulsion droplets are more stable to coalescence in brine than in DI, together with extended DLVO theory, supports the formation of the particle networks described in literature. As shown in Fig. 1(b), with sufficiently high ionic concentrations in brine screening electrostatic forces, unattached particles in the aqueous phase are slightly attracted by van der Waals forces outside of the range of steric repulsion. These particles interact and form aggregate networks between the emulsion droplets that likely lead to the increased stability observed from our experiments of emulsions in brine. Particle networks were previously observed in a similar GLYMO-NP-Brine system with cryo-SEM imaging [33]. By freezing the emulsion droplets, the authors were able to capture images of white threads (representing dense nanoparticle connections) connecting their emulsion droplets. This process is illustrated in Fig. 6. Given the catastrophic loss of stability of our GLYMO-NP-5API emulsions with 0.1 wt% nanoparticles under ordinary gravity, these networks likely formed for our 50% decane emulsions at a critical concentration between 0.1 and 0.2 wt% nanoparticles. Interestingly, as observed in Fig. 4, the presence of unfiltered GLYMO appeared to completely destabilize these networks.

We can quantify the added stability particle networks contribute to emulsions based on the measured coalescence and D_{32} diameters. GLYMO-NP-DI exhibited a similar stability profile to GLYMO-NP-5API at 4.3 ± 0.5 times smaller D_{32} diameters. Because the orthokinetic rate constant for the coalescence of spherical drops is proportional to the cube of the droplet diameter [28], we calculate that brine-stabilized particle networks reduced the rate constant by a factor of 78 ± 23, relative to dissociated particles in deionized water. In contrast to other work that examines the presence of particle networks [31–34], this finding provides a direct quantification of the impact of particle networks on the coa-

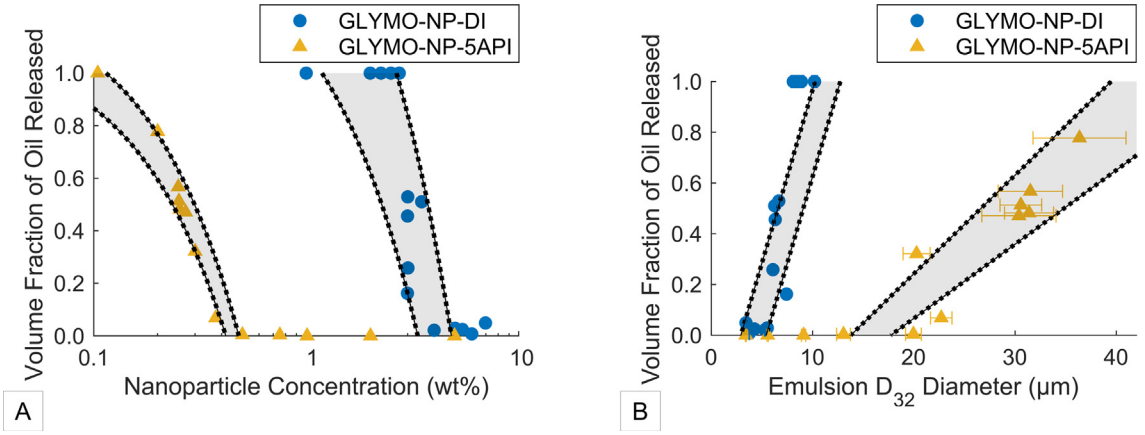

Fig. 5. Volume fraction of oil released during centrifugation for filtered GLYMO-NP emulsions in DI and 5API brine as a function of (a) nanoparticle mass concentration on a log scale or (b) emulsion D_{32} diameter in microns. The shaded region represents two standard deviations of uncertainty in the volume fraction of oil released around a linear fit to the data.

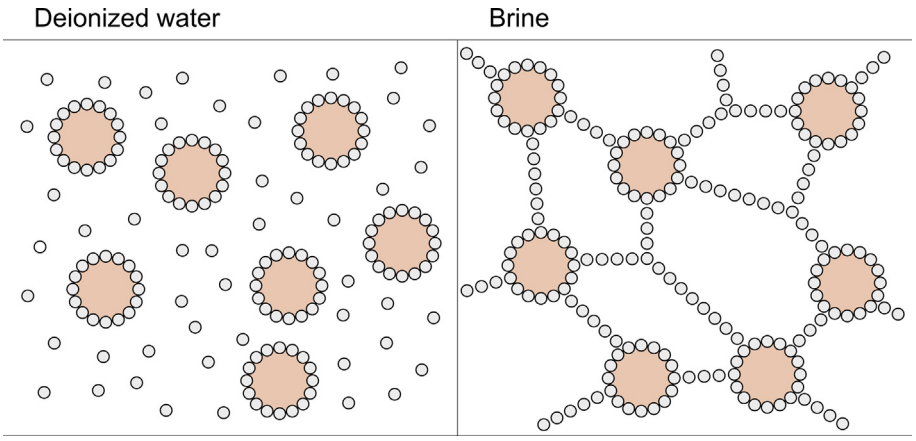

Fig. 6. Predicted behavior of nanoparticles dispersed in the continuous phase in a Pickering emulsion. In deionized water, the unattached particles repel and remain dissociated. In brine, the particles attract, forming inter-droplet particle networks.

lescence of Pickering emulsions in response to compressive forces, accounting for changes in droplet diameter.

4. Conclusions

We measured the relative dynamic stability of GLYMO-NP emulsions over a range of controlled conditions. We found that GLYMO-NP in 5API brine generated smaller, more stable emulsions than in DI. By increasing nanoparticle concentration from 0.2 wt% to 5 wt%, we observed D_{32} diameters of brine emulsion droplets decrease from 36 ± 5 μm to 3.41 ± 0.05 μm. The D_{32} diameters of DI emulsion droplets decreased from 10.2 ± 0.3 μm to 3.42 ± 0.02 as nanoparticle concentration increased from 2 wt% to 7 wt%. At the overlapping concentration range of 2 wt% to 5 wt%, emulsion droplets in DI and brine exhibited droplet diameters ranging from 10.2 ± 0.3 μm to 5.52 ± 0.02 μm and 5.57 ± 0.07 μm to 3.41 ± 0.0 5 μm, respectively; controlling for nanoparticle concentration, DI emulsion droplets were 50–80% larger than brine emulsion droplets. The brine emulsions exhibited greater stability, matching the coalescence profile of DI emulsions with 12 times more nanoparticles in dispersion. Controlling for the change of droplet size, the brine emulsions demonstrated the same stability as DI emulsions with 4.3 ± 0.5 times smaller diameters. Based on the effect of diameter on the orthokinetic constant, this result suggests that particle networks slowed the rate of coalescence by a factor of 78 ± 23. These trends were not present in emulsions with unfiltered particles.

These findings help quantify results from past work showing a link between increased salinity and higher emulsion stability [22,24,27–30]. We applied centrifugation methods for determining dynamic emulsion stability [22–24] over a wider particle concentration range in both DI and brine, enabling us to quantify clear stability thresholds for DI and brine emulsions that were similar in behavior but an order of magnitude apart in particle concentration. We found that emulsion stability was highly sensitive to particle concentration, and that high-salinity nanoparticle interactions contributed as much to emulsion stability as a twelvefold increase in particle concentration. We further expanded on droplet diameter observations in past studies [22,27,28,30] with detailed microscopy measurements over a large range of particle concentrations to infer the effect of DLVO interactions on droplet formation and control for effects of droplet size. The smaller droplet diameters of brine emulsions indicated that the nanoparticles packed more closely during sonication, creating tighter layers at the droplet interface. The diameters of both brine and DI emulsions deviated from geometric predictions at higher particle concentrations, suggesting a tradeoff between the number of particles and sonication efficiency. Based on these droplet diameters, we were able to quantify the extra emulsion stability granted by salinity when controlling for these differences. These results highlight the importance of salinity-dependent particle interactions to both emulsion formation and stability, and are relevant to applications in porous media where salinity is often high. To further examine the role of ligands on nanoparticle bridging, future work will investigate the effect of ligand concentration at the nanoparticle surface on particle interactions and emulsion stability.

CRediT authorship contribution statement

Daniel Hatchell: Conceptualization, Methodology, Validation, Formal analysis, Investigation, Writing – original draft, Visualization. **Wen Song:** Conceptualization, Methodology, Writing – review & editing. **Hugh Daigle:** Conceptualization, Methodology, Resources, Writing – review & editing, Supervision, Project administration, Funding acquisition.

Declaration of Competing Interest

The authors declare that they have no known competing financial interests or personal relationships that could have appeared to influence the work reported in this paper.

Acknowledgements

The authors would like to thank Hugo Celio and Raluca Gearba for their assistance with running experiments on DLS and TGA. This work was supported by assistance from Nyacol Nano Technologies, who supplied nanoparticles. This material is based upon work supported by the National Science Foundation Graduate Research Fellowship Program under Grant No. (DGE-1610403). Any opinions, findings, and conclusions or recommendations expressed in this material are those of the authors and do not necessarily reflect the views of the National Science Foundation. This work was further supported by the Nanoparticles for Subsurface Engineering Industrial Affiliates Program (member companies Nissan Chemical of America, Baker Hughes, and Foundation CMG) at the University of Texas at Austin.

Appendix A. Supplementary material

Supplementary data to this article can be found online at https://doi.org/10.1016/j.jcis.2021.10.154.

References

[1] Y. Chevalier, M.-A. Bolzinger, Emulsions stabilized with solid nanoparticles: Pickering emulsions, Colloids Surf., A: Physicochem. Eng. Aspects 439 (2013) 23–34.
[2] J. Wu, G.-H. Ma, Recent studies of Pickering emulsions: particles make the difference, Small 12 (34) (2016) 4633–4648.
[3] Y. Yang, Z. Fang, X. Chen, W. Zhang, Y. Xie, Y. Chen, Z. Liu, W. Yuan, An overview of Pickering emulsions: solid-particle materials, classification, morphology, and applications, Front. Pharmacol. 8 (2017), https://doi.org/10.3389/fphar.2017.00287.
[4] D. Arab, A. Kantzas, S.L. Bryant, Nanoparticle stabilized oil in water emulsions: A critical review, J. Petrol. Sci. Eng. 163 (2018) 217–242.
[5] R.D. Kaminsky, R.C. Wattenbarger, J. Lederhos, S.A. Leonardi, January). Viscous oil recovery using solids-stabilized emulsions, Society of Petroleum Engineers, 2010.
[6] J.R. Bragg. *U.S. Patent No. 5,855,243*. Washington, DC: U.S. Patent and Trademark Office, 1999.
[7] S. Ko, E.S. Kim, S. Park, H. Daigle, T.E. Milner, C. Huh, M.V. Bennetzen, G.A. Geremia, Amine functionalized magnetic nanoparticles for removal of oil droplets from produced water and accelerated magnetic separation, J. Nanopart. Res. 19 (4) (2017) 132.
[8] W. Ramsden, Separation of solids in the surface-layers of solutions and 'suspensions' (observations on surface-membranes, bubbles, emulsions, and mechanical coagulation).—Preliminary account, Proc. Roy. Soc. London 72 (477–486) (1904) 156–164.
[9] S.U. Pickering, Cxcvi.—emulsions, J. chem. Soc. Trans. 91 (0) (1907) 2001–2021.
[10] S. Levine, B.D. Bowen, S.J. Partridge, Stabilization of emulsions by fine particles I. Partitioning of particles between continuous phase and oil/water interface, Colloids Surf. 38 (2) (1989) 325–343.
[11] B.P. Binks, J.H. Clint, Solid wettability from surface energy components: relevance to Pickering emulsions, Langmuir 18 (4) (2002) 1270–1273.
[12] C.D. McAuliffe, Oil-in-water emulsions and their flow properties in porous media, J. Petrol. Technol. 25 (06) (1973) 727–733.
[13] H. Soo, C.J. Radke, Flow mechanism of dilute, stable emulsions in porous media, Ind. Eng. Chem. Fundam. 23 (3) (1984) 342–347.
[14] I. Kim, A.J. Worthen, M. Lotfollahi, K.P. Johnston, D.A. DiCarlo, C. Huh, April). Nanoparticle-stabilized emulsions for improved mobility control for adverse-mobility waterflooding Vol. 2017(1 (2017) 1–13.
[15] G.J. Lee, H.A. Son, J.W. Cho, S.K. Choi, H.T. Kim, J.W. Kim, Stabilization of Pickering emulsions by generating complex colloidal layers at liquid–liquid interfaces, J. Colloid Interface Sci. 413 (2014) 100–105.
[16] R. Aveyard, B.P. Binks, J.H. Clint, Emulsions stabilised solely by colloidal particles, Adv. Colloid Interface Sci. 100-102 (2003) 503–546.
[17] J. Frelichowska, M.-A. Bolzinger, Y. Chevalier, Pickering emulsions with bare silica, Colloids Surf., A 343 (1-3) (2009) 70–74.
[18] F. Nan, J. Wu, F. Qi, Y. Liu, T.o. Ngai, G. Ma, Uniform chitosan-coated alginate particles as emulsifiers for preparation of stable Pickering emulsions with stimulus dependence, Colloids Surf., A 456 (2014) 246–252.
[19] F. Yang, S. Liu, J. Xu, Q. Lan, F. Wei, D. Sun, Pickering emulsions stabilized solely by layered double hydroxides particles: The effect of salt on emulsion formation and stability, J. Colloid Interface Sci. 302 (1) (2006) 159–169.
[20] N.M. Briggs, J.S. Weston, B. Li, D. Venkataramani, C.P. Aichele, J.H. Harwell, S.P. Crossley, Multiwalled carbon nanotubes at the interface of Pickering emulsions, Langmuir 31 (48) (2015) 13077–13084.
[21] S. Maaref, A. Kantzas, S.L. Bryant, The effect of silanization assisted nanoparticle hydrophobicity on emulsion stability through droplet size distribution analysis, Chem. Eng. Sci. 201 (2019) 175–190.
[22] C. Griffith, H. Daigle, A comparison of the static and dynamic stability of Pickering emulsions, Colloids Surf., A 586 (2020) 124256.
[23] J. Frelichowska, M.-A. Bolzinger, Y. Chevalier, Effects of solid particle content on properties of o/w Pickering emulsions, J. Colloid Interface Sci. 351 (2) (2010) 348–356.
[24] A. Saha, A. Nikova, P. Venkataraman, V.T. John, A. Bose, Oil emulsification using surface-tunable carbon black particles, ACS Appl. Mater. Interfaces 5 (8) (2013) 3094–3100.
[25] P.M. Kruglyakov, A.V. Nushtayeva, N.G. Vilkova, Experimental investigation of capillary pressure influence on breaking of emulsions stabilized by solid particles, J. Colloid Interface Sci. 276 (2) (2004) 465–474.
[26] L. Maurice, R.A. Maguire, A.B. Schofield, M.E. Cates, P.S. Clegg, J.H. Thijssen, Squeezing particle-stabilized emulsions into biliquid foams–equation of state, Soft Matter 9 (32) (2013) 7757–7765.
[27] S. Varanasi, L. Henzel, L. Mendoza, R. Prathapan, W. Batchelor, R. Tabor, G. Garnier, Pickering emulsions electrostatically stabilized by cellulose nanocrystals, Front. Chem. 6 (2018) 409.
[28] C.P. Whitby, F.E. Fischer, D. Fornasiero, J. Ralston, Shear-induced coalescence of oil-in-water Pickering emulsions, J. Colloid Interface Sci. 361 (1) (2011) 170–177.
[29] W. Song, A.R. Kovscek, Functionalization of micromodels with kaolinite for investigation of low salinity oil-recovery processes, Lab Chip 15 (16) (2015) 3314–3325.
[30] W. Song, A.R. Kovscek, Spontaneous clay Pickering emulsification, Colloids Surf., A 577 (2019) 158–166.
[31] S.R. Raghavan, J. Hou, G.L. Baker, S.A. Khan, Colloidal interactions between particles with tethered nonpolar chains dispersed in polar media: direct correlation between dynamic rheology and interaction parameters, Langmuir 16 (3) (2000) 1066–1077.
[32] T.S. Horozov, B.P. Binks, T. Gottschalk-Gaudig, Effect of electrolyte in silicone oil-in-water emulsions stabilised by fumed silica particles, PCCP 9 (48) (2007) 6398–6404.
[33] C. Griffith, H. Daigle, Manipulation of Pickering emulsion rheology using hydrophilically modified silica nanoparticles in brine, J. Colloid Interface Sci. 509 (2018) 132–139.
[34] D.J. French, P. Taylor, J. Fowler, P.S. Clegg, Making and breaking bridges in a Pickering emulsion, J. Colloid Interface Sci. 441 (2015) 30–38.
[35] A.J. Worthen, V.u. Tran, K.A. Cornell, T.M. Truskett, K.P. Johnston, Steric stabilization of nanoparticles with grafted low molecular weight ligands in highly concentrated brines including divalent ions, Soft Matter 12 (7) (2016) 2025–2039.
[36] American Petroleum Institute (1960). Recommended practice standard procedure for the evaluation of hydraulic fracturing fluids. *API RP, 39*(1st Edition).
[37] L.T. Zhuravlev, Concentration of hydroxyl groups on the surface of amorphous silicas, Langmuir 3 (3) (1987) 316–318.
[38] B.P. Binks, S.O. Lumsdon, Stability of oil-in-water emulsions stabilised by silica particles, PCCP 1 (12) (1999) 3007–3016.
[39] C.O. Metin, J.R. Baran, Q.P. Nguyen, Adsorption of surface functionalized silica nanoparticles onto mineral surfaces and decane/water interface, J. Nanopart. Res. 14 (11) (2012) 1246.
[40] B. Derjaguin, L. Landau, The theory of stability of highly charged lyophobic sols and coalescence of highly charged particles in electrolyte solutions, Acta Physicochim. URSS 14 (633–52) (1941) 58.
[41] E.J.W. Verwey, J.T.G. Overbeek, K. Van Nes, Theory of the stability of lyophobic colloids: the interaction of sol particles having an electric double layer, Elsevier Publishing Company, 1948.
[42] J.N. Israelachvili, Intermolecular and surface forces, Academic press, 2011.
[43] I. Luzinov, D. Julthongpiput, A. Liebmann-Vinson, T. Cregger, M.D. Foster, V.V. Tsukruk, Epoxy-terminated self-assembled monolayers: molecular glues for polymer layers, Langmuir 16 (2) (2000) 504–516.
[44] H. Chen, A.Z. Panagiotopoulos, Communication: Modeling electrolyte mixtures with concentration dependent dielectric permittivity, J. Chem. Phys. 148 (4) (2018) 041102, https://doi.org/10.1063/1.5018195.
[45] B. Vincent, J. Edwards, S. Emmett, A. Jones, Depletion flocculation in dispersions of sterically-stabilised particles ("soft spheres"), Colloids Surf. 18 (2-4) (1986) 261–281.
[46] S. Maaref, S. Ayatollahi, The effect of brine salinity on water-in-oil emulsion stability through droplet size distribution analysis: a case study, J. Dispersion Sci. Technol. 39 (5) (2018) 721–733.